Catalysis Science & Technology

Accepted Manuscript

This article can be cited before page numbers have been issued, to do this please use: A. Osatiashtiani, S. A. Orr, L. Durndell, I. Collado García, A. Merenda, A. F. Lee and K. Wilson, *Catal. Sci. Technol.*, 2022, DOI: 10.1039/D2CY00538G.

ROYAL SOCIETY OF CHEMISTRY

rsc.li/catalysis

View Article Online
DOI: 10.1039/D2CY00538G

ARTICLE

Liquid phase catalytic transfer hydrogenation of ethyl levulinate to γ-valerolactone over ZrO_2/SBA-15

Received 00th January 20xx,
Accepted 00th January 20xx

DOI: 10.1039/x0xx00000x

Amin Osatiashtiani,[a] Samantha A. Orr,[b] Lee J. Durndell,[c] Irene Collardo Garcia,[a,d] Andrea Merenda,[b] Adam F. Lee*[b] and Karen Wilson*[b]

γ-Valerolactone (GVL) is an important bio-derived platform molecule whose atom- and energy efficient, and scalable, catalytic synthesis is highly desirable. Catalytic transfer hydrogenation (CTH) of ethyl levulinate (EL) to γ-valerolactone (GVL) has been selectively performed in batch and continuous flow over ZrO_2/SBA-15 solid acid catalysts. Tuning the zirconia adlayer delivered maximum CTH activity for 11.6 wt% Zr, ascribed to the optimal ratio of Lewis and Brønsted acid sites for the two-step cascade reaction. EL conversion almost doubled under flow versus batch operation, accompanied by a small rise in selectivity to GVL, tripling average GVL productivity in continuous flow (5.2 vs 1.37 mmol $g^{-1}.h^{-1}$). Turnover frequency (TOF) is significantly improved under flow conditions (14.5 h^{-1}) relative to batch (3.6 h^{-1}), demonstrating the utility of flow chemistry for accelerating the manufacture of valuable bio-derived molecules.

Introduction

Climate change mitigation, through reduced Greenhouse Gas emissions and innovative renewable energy technologies, is a global scientific endeavour. Meeting this challenge requires carbon neutral resources to eliminate current reliance on fossil sources of chemicals and fuels. Biomass is a promising, low cost and abundant renewable carbon source whose exploitation could offer an array of valuable platform chemicals[1, 2] either as direct replacements for existing petrochemicals or as molecules and materials with unique properties. Lignocellulosic biomass, as a non-food biomass feedstock, is of particular interest for the production of monosaccharides and phenolics, and their subsequent transformation to biofuels and bio-derived chemicals (Scheme 1).[3, 4] One such product is the platform chemical γ-valerolactone (GVL) due to its desirable physicochemical properties, notably low vapour pressure, high boiling point (~207 °C) and water solubility.[5, 6] This versatile cyclic ester is a naturally occurring, non-toxic and biodegradable molecule, with potential commercial application as a food and fuel additive (for gasoline) and green solvent.[7-11] Industrially relevant GVL-derived products include alkanes, methyl-tetrahydrofuran, α-methylene-γ-valerolactone monomer[12] and valeric esters, for use in the energy, chemical and plastic manufacturing sectors.

GVL can be obtained from various biomass-derived precursors, including furfural[13-15] and cellulose,[16] however it is usually produced by the reduction of levulinic acid (LA) and its alkyl levulinate ester (Scheme 1).[6, 17] Catalytic hydrogenation of bio-derived LA and alkyl levulinates to yield GVL often employs molecular hydrogen, noble metal catalysts[6, 18-20] and high operating pressures (>30 bar), which are uneconomical and hinder process scale-up. Over the past decade, catalytic transfer hydrogenation (CTH), exploiting formic acid[21] or an alcohol[22] as the hydrogen source, has emerged as a more promising route from LA to GVL. Pioneering work by Dumesic and coworkers[23] demonstrated that CTH followed a Meerwein-Pondorf-Verley (MPV) mechanism. A secondary alcohol (typically isopropanol) is the preferred hydrogen donor, with heterogeneous ZrO_2 catalysts active for GVL production in batch and vapour flow reactors, eliminating the need for Earth scare precious metals and harsh reaction conditions.

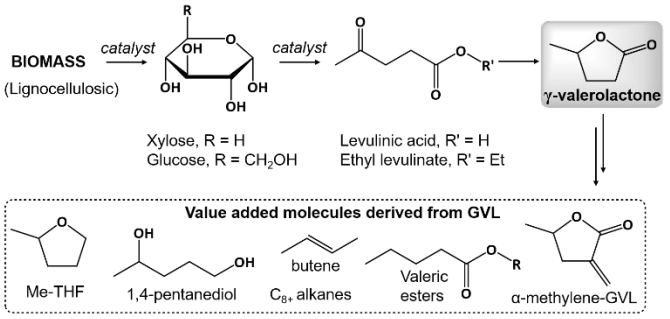

Scheme 1. Summary synthesis of GVL and its derivatives from lignocellulosic biomass.

Mechanistically, there are three major catalytic pathways from LA to GVL: (i) hydrogenation to a 4-hydroxyvaleric acid intermediate and subsequent dehydration; (ii) dehydration to α-angelica lactone followed by hydrogenation; and (iii) esterification to an alkyl levulinate and subsequent hydrogenation and cyclisation. The second pathway typically affords lower GVL yields due to catalyst coking and deactivation arising from the oligomerisation of α-angelica lactones.[6, 24] Recent studies have investigated GVL production from alkyl

[a] EBRI, Aston University, Birmingham B4 7ET, UK.
[b] Centre for Advanced Materials and Industrial Chemistry, RMIT University, Melbourne VIC3000, Australia.
[c] School of Geography, Earth and Environmental Sciences, University of Plymouth, Plymouth PL4 8AA, UK.
[d] ACERINOX, S.A, 11379 Los Barrios, Cádiz, Spain.
Electronic Supplementary Information (ESI) available: additional catalyst characterisation and reaction data. See DOI: 10.1039/x0xx00000x

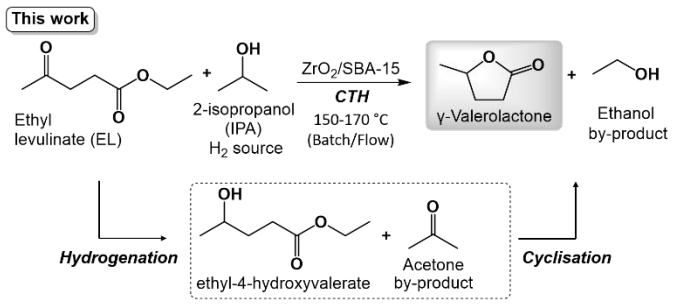

Scheme 2. Catalytic transfer hydrogenation (CTH) of EL with 2-isopropanol.

levulinates through a cascade hydrogenation-cyclisation pathway (**Scheme 2**), wherein the cyclisation of 4-hydroxy-valeric ester intermediates (such as ethyl 4-hydroxyvalerate) and concomitant alcohol loss yields higher selectivity to GVL.[6, 23-27]

A range of zirconia materials are reported for CTH of LA and alkyl levulinates to GVL, including ZrO_2 nanoparticles,[24, 25, 27] zirconium hydroxide,[28] and Zr-SBA-15 and ZrO_2/SBA-15 coated mesoporous silica scaffolds.[27] As an Earth abundant and low cost metal, with amphoteric properties, zirconia is attractive for MPV reductions wherein Lewis acid and base sites may act in concert to effect the reduction of carbonyls by direct hydrogen transfer. CTH of alkyl levulinates over ZrO_2, ZrO_2/SBA-15 and ZrO_2/graphene oxide has been investigated in batch reactors, typically operating between 150-250 °C and 10-20 bar autogeneous pressure. ZrO_2/SBA-15 and nanoparticulate ZrO_2 can achieve time-averaged GVL productivities spanning 1.49-5.2 $mmol.g^{-1}.h^{-1}$,[23, 24, 26] being higher for the latter, although an improved productivity of 9.8 $mmol.g^{-1}.h^{-1}$ is reported at 180 °C for zirconia supported on graphene oxide.[29]

Continuous flow chemistry offers great control over reaction parameters, and hence optimisation of reactant conversion and product selectivity, in addition to improved safety, atom-efficiency and waste minimisation. Flow chemistry is also amenable to rapid scale-up and hence suited to large-scale biorefinery operation.[30, 31] Continuous flow reactors have been applied to CTH of alkyl levulinates to GVL, notably methyl- and butyl- levulinate (ML and BL) in the liquid phase[23, 27] and methyl- and ethyl- levulinate (ML and EL) in the vapour phase.[24, 25, 32] Under forcing conditions of 200 °C and 30 bar, an average liquid phase GVL productivity of 34.2 $mmol.g^{-1}.h^{-1}$, and corresponding turnover frequency (TOF) of 133 h^{-1}, were attained from ML over ZrO_2/SBA-15.[27] In contrast, ZrO_2 catalysed CTH of EL to GVL in the vapour phase at 250 °C achieved an average GVL productivity and TOF of 0.049 $mmol.g^{-1}.h^{-1}$ and 1.38 h^{-1} respectively, albeit this poorer performance may reflect mass-transport limitations due to operation at complete EL conversion.[24] The direct hydrogenation of EL to GVL in a continuous gas/liquid flow reactor is reported over Ru/C,[33] however, in addition to the complexity and hazards of 100 bar H_2 operation at scale, the resulting GVL selectivity was ≤50 %. Despite the promising preliminary results for liquid phase flow conversion of ML and BL to GVL over ZrO_2 catalysts,[23, 27] to the best of our knowledge the corresponding transformation of EL to GVL remains unexplored.

Herein, we examine the reactivity of ZrO_2/SBA-15 catalysts, and role of their surface acidity, in the batch and continuous liquid phase CTH of EL to GVL. Optimising the zirconia loading and hence Brønsted:Lewis acid ratio maximises the GVL yield in batch, with flow operation further enhancing activity by suppressing blocking of active sites by the strongly adsorbing, reactively-formed GVL product.

Experimental

Catalyst preparation

ZrO_2-grafted SBA-15 was synthesised according to our previous report.[34] Briefly, 2 g of SBA-15 (prepared via the original method of Zhao et al.[35]) was dried at 300 °C for 4 h, then cooled to 100 °C and added to 60 mL of anhydrous hexane (Sigma, 95 %). An appropriate amount of $Zr(OCH_2CH_2CH_3)_4$ solution (Sigma, 70 wt% in propanol) was then added to the slurry under a nitrogen atmosphere and magnetic stirring. The amount of zirconium precursor was calculated from the number of surface hydroxyls on the SBA-15 support determined by thermogravimetric analysis (TGA). Dry solvent ensured that $Zr(OCH_2CH_2CH_3)_4$ only reacts with surface hydroxyls, promoting growth of a conformal adlayer over SBA-15. The slurry was refluxed under stirring at 69 °C overnight, filtered, and washed three times with dry hexane to remove any unreacted precursor. The material was subsequently reacted with 60 mL of deionised water under stirring for 4 h to fully hydrolyse the residual surface propoxide groups. Finally, the catalyst was filtered and dried at 80 °C overnight, and then activated by calcination at 550 °C in static air for 3 h to obtain a white powder.

Catalyst characterisation

Physicochemical properties of catalysts were fully characterised. Surface areas and pore sizes were measured by N_2 physisorption on a Quantasorb Nova 4000 instrument, after sample outgassing at 120 °C for 4 h prior to analysis at -196 °C. Surface areas were calculated using the Brunauer–Emmett–Teller (BET) method over the range P/P_0 = 0.4–0.8, where a linear relationship was maintained. Pore size distributions were calculated using the Barrett–Joyner–Halenda (BJH) model applied to the desorption branch of the isotherm. Structural order was evaluated by low angle X-ray powder diffraction (XRD) on a Bruker D8 Advance diffractometer using Cu K_α radiation between 2θ =0.6-5.0° with a step size of 0.02°. Crystalline phase identification was performed by wide angle XRD between 2θ=10-80° with a step size of 0.04°. Diffuse reflectance infra-red Fourier transform (DRIFT) spectra were obtained using a Thermo Scientific Nicolet environmental cell and smart collector accessory on a Thermo Scientific Nicolet iS50 FT-IR Spectrometer with MCT detector. Samples were homogeneously diluted to 10 wt% with KBr and loaded into a Nicolet Avatar 370 MCT with Smart Collector accessory prior to evacuation at 200 °C for 2 h to remove physisorbed water; analysis was performed at 200 °C. Ex-situ pyridine adsorption was performed by adding pyridine (Sigma, 99 %) to diluted samples (10 wt% in KBr) until wet. Excess physisorbed pyridine was removed in vacuo at 50 °C

overnight prior to recording in vacuo DRIFT spectra at 50 °C in the Smart Collector environmental cell. Acid site loading was determined by propylamine adsorption and subsequent TGA-mass spectrometry (MS) analysis. Catalysts were wetted with propylamine, with excess physisorbed propylamine removed in vacuo at room temperature prior to temperature programmed desorption on a Mettler Toledo TGA/DSC 2 STARe System equipped with a Pfeiffer Vacuum ThermoStarTM GSD 301 T3 mass spectrometer. Evolution of reactively-formed propene (m/z=41 amu) evidenced acid catalysed propylamine decomposition, with lower temperature desorption indicative of stronger acid sites.

Catalytic reactions

General procedure for batch reactions: Catalytic transfer hydrogenation was performed in a 50 mL stainless steel Parr autoclave, using 250 mmol (19.1 mL) of 2-isopropanol as solvent and hydrogen donor, 5 mmol (0.72 g) ethyl levulinate, 0.5 mmol (0.09 g) dodecane as internal standard and 100 mg catalyst. The reactor was charged with reactants and catalyst at room temperature, and then purged with N_2 and pressurised to 5 bar and heated without stirring to the desired reaction temperature (typically 170 °C). Stirring then commenced at 500 rpm, and aliquots of the reaction mixture periodically removed via a dip-tube in the solution, filtered to remove catalyst, and analysed using a Shimadzu GC-2010Plus equipped with WAXPlus column and flame ionisation detector (FID).

General procedure for flow reactions: Continuous flow catalytic transfer hydrogenation of EL and 2-isopropanol was conducted at 150 °C using a Uniqsis FlowSyn reactor. 100 mg catalyst was diluted with quartz beads (Sigma, mesh size = 325), and packed within a 10 mm i.d. × 100 mm OMNIFIT® glass column to give a total bed length of between 3.5 to 4 cm^3. A liquid stream of 2-isopropanol (250 mmol) and EL (5 mmol) was delivered to the packed bed at flow rates between 0.1 to 0.18 $ml.min^{-1}$. Samples were periodically collected for GC analysis.

Results and discussion

Catalyst characterisation

Synthesis and characterisation of ZrO_2 grafted SBA-15 catalysts (0.8-14.6 wt% Zr loading) by N_2 physisorption, TEM and XRD in agreement with our previous report.[34] Bulk and surface Zr contents of each catalyst were determined by ICP-OES and XPS (**Figure S1-2, Table S1**), respectively. Textural properties are summarised in **Table 1**, with N_2 porosimetry revealing type IV isotherms and H1 hysteresis loops (**Figure S3**) in all cases, characteristic of the parent SBA-15 and confirming retention of the mesoporous silica framework after ZrO_2 grafting. BET surface areas, pore volumes and mean mesopore diameters are consistent with layer-by-layer growth of conformal ZrO_2 adlayers (**Table 1**). Complementary TEM imaging (**Figure S4**) revealed hexagonal (*p6mm*) ordering of parallel mesopore channels for the parent SBA-15 support, and the absence of any higher contrast zirconium features. Low angle XRD patterns exhibited peaks at 2θ = 1.0, 1.7 and 1.9°, assigned to the (100), (110) and (200) reflections of the mesoporous silica support (**Figure S5a**).[35] Wide angle powder XRD confirmed the absence of crystalline ZrO_2 nanoparticles, consistent with the uniform deposition of a highly dispersed zirconium phase throughout the SBA-15 mesopore network.

The strength and nature of catalyst acidity are fundamental to their corresponding reactivity towards the transformation of EL to GVL. Surface acidity was analysed by propylamine temperature programmed desorption (PA-TPD) and pyridine-DRIFTS (**Figure S6-7**) to identify the respective acid strength and Lewis/Brønsted acid character. Integrating the reactively-desorbed propene desorption (**Figure 1**) between 320-500 °C yields the total surface acidity for ZrO_2/SBA-15. Acid loadings increased with Zr content before reaching a plateau at 11.6 wt%, indicative of a complete monolayer[34] (**Table 1**). The propene desorption peak maximum, and hence strength of surface acid sites, was approximately independent of Zr loading.

The nature of acid sites was examined by DRIFTS of chemisorbed pyridine (**Figure 2a**). Bands at 1445, 1490 and

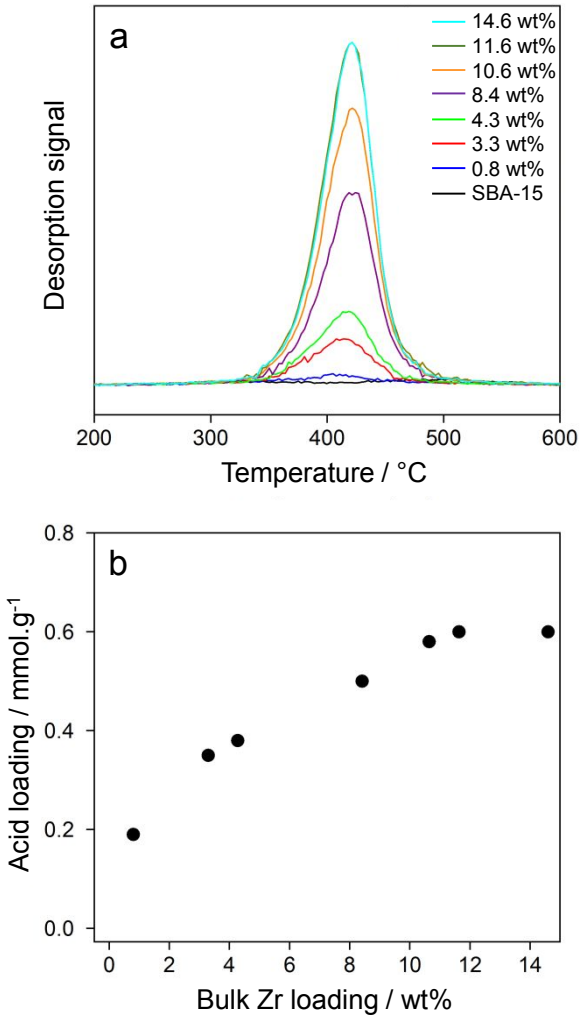

Figure 1. (a) Temperature-programmed desorption of reactively-formed propene (41 amu) from propylamine decomposition, and (b) corresponding acid site loading dependence on Zr content of ZrO_2/SBA-15.

View Article Online
DOI: 10.1039/D2CY00538G

Table 1. Physicochemical properties of ZrO_2/SBA-15.

Zr loading[a] / wt%	S_{BET}[b] / $m^2\ g^{-1}$	V_p[c] / $cm^3\ g^{-1}$	D_p[d] / nm	Acid loading / mmol g^{-1}	Lewis acid loading / mmol g^{-1}	Brønsted acid loading / mmol g^{-1}	Brønsted:Lewis ratio
0	789	1.08	5.9	-	-	-	-
0.8	731	0.97	5.8	0.19	0.19	0.00	0
3.3	761	1.02	5.8	0.35	0.33	0.02	0.06
4.3	659	0.89	5.8	0.38	0.34	0.04	0.12
8.4	642	0.88	5.8	0.50	0.44	0.06	0.14
10.6	662	0.92	5.9	0.58	0.45	0.13	0.28
11.6	602	0.86	5.8	0.60	0.48	0.12	0.26
14.6	581	0.80	5.8	0.60	0.51	0.09	0.17

[a]ICP-OES. [b]N_2 porosimetry. [c]Total pore volume for P/P_0 = 0.4– 0.8. [d]Mean pore size from BJH method.

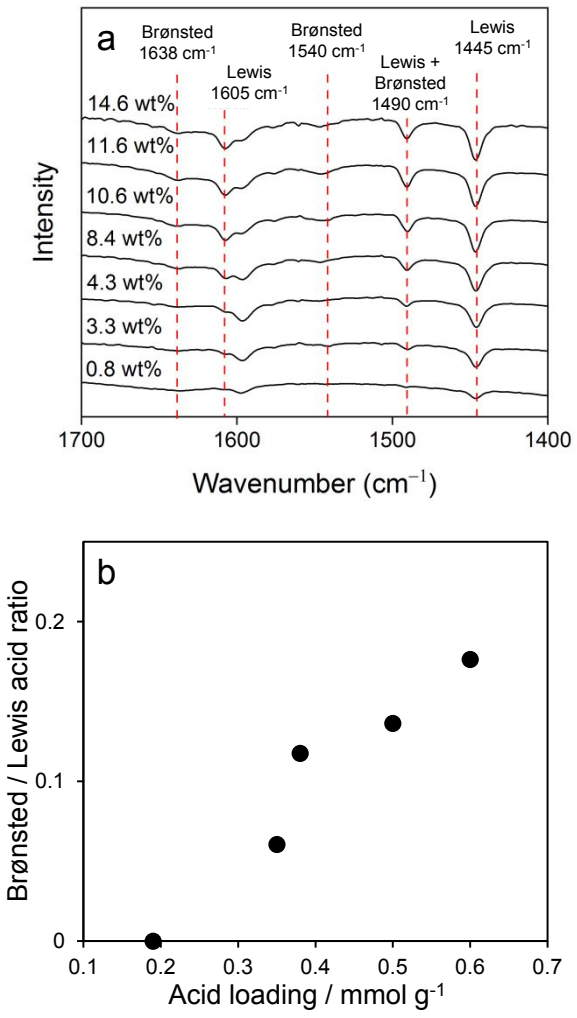

Figure 2. (a) Pyridine-DRIFTS spectra, and (b) corresponding Brønsted:Lewis acid intensity ratio of ZrO_2/SBA-15.

1605 cm^{-1} are attributed to pyridine bound to Lewis acid sites, and those at 1490, 1540 and 1638 cm^{-1} to pyridinium ions coordinated to Brønsted acid sites.[14] Lewis acidity was proportional to Zr loading (**Figure 2b**), whereas Brønsted acidity reached a plateau upon ZrO_2 monolayer completion (>10.6 wt% Zr). Formation of Brønsted sites on Zr/SBA-15 is attributed to surface silanols in proximity to zirconia.[14] A ZrO_2 monolayer on SBA-15 exhibited predominantly Lewis acidity but still possessed significant Brønsted acidity.

Batch synthesis of γ-valerolactone from ethyl levulinate

The batchwise performance of ZrO_2/SBA-15 catalysts for the transformation of EL to GVL was initially studied in 2-isopropanol at 170 °C to identify the optimum Zr loading (**Figure S8-10**). EL conversion increased monotonically with acid loading up to completion of the ZrO_2 monolayer (**Figure 3a**), reaching ~55 % after 6 h. Corresponding GVL selectivity at ~13 % isoconversion also showed a strong dependence on acid loading, with a maximum of ~70 % for the ZrO_2 monolayer. The observation that maximum ester conversion obtains for ~10 wt% Zr coincides with that reported by Kuwahara et al. for ML over ZrO_2/SBA-15 (prepared by an analogous synthesis using $Zr(O^nBu)_4$), albeit they only investigated high Zr loadings spanning 10-60 wt%.[26] GC-MS and ^1H NMR analysis confirmed GVL and isopropyl levulinate (product of competitive transesterification **Scheme 3**) as the sole reaction products, with no angelica lactones formed (**Figure S11-12**). The rise in GVL selectivity for high acid loadings likely reflects increased Brønsted acidity and concomitant enhanced cyclisation of valeric intermediates. Corresponding turnover frequency (TOF) and GVL productivity, normalised to total acid site loadings and calculated during the first 2 h of reaction (**Figure 3b**), mirror the trends in conversion and selectivity. As the strength of acid sites is loading invariant, the increase in TOF suggests either improved accessibility of Lewis acid sites for EL conversion as the ZrO_2 adlayer spreads across the silica substrate, the genesis of more active CTH sites, or the emergence of competing reactions such as Brønsted acid catalysed EL transesterification (**Scheme 3**).[26] The latter is discounted since both GVL selectivity and productivity increase with acid loading. Growth of a 2D zirconia adlayer should not improve accessibility to zirconium active sites since their dispersion can only decrease as isolated Zr(IV) centres aggregate into ZrO_2 islands. The increase in TOF with Zr content (acid site loading) is therefore attributed to the emergence of cooperativity between Lewis acid-base pairs and Brønsted sites. The surface termination of zirconia is a function of phase and particle size, with the formation and coupling of unsaturated Zr^{4+} Lewis acid sites to adjacent basic O^{2-} species

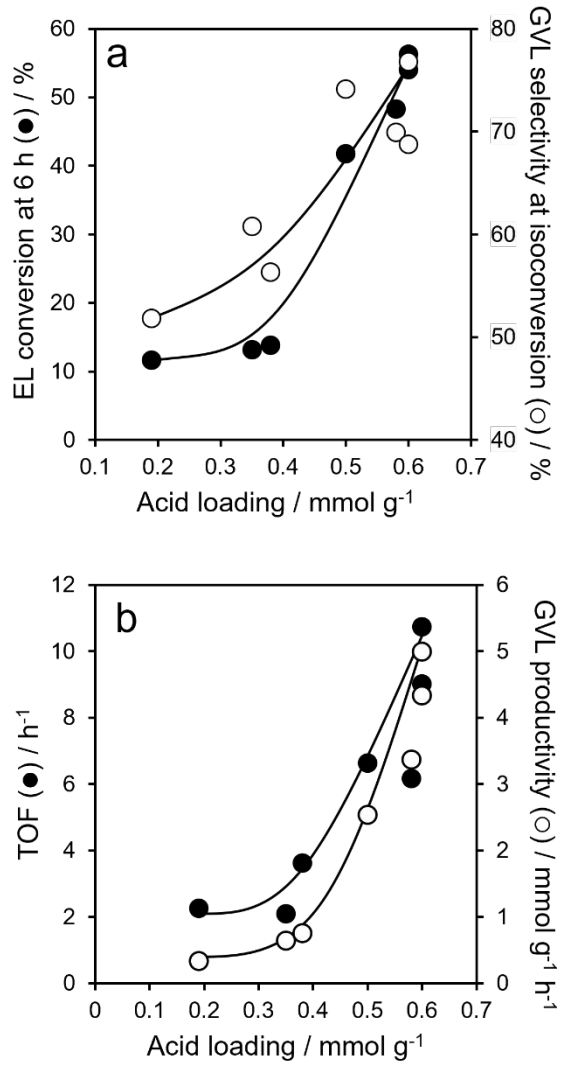

Figure 3. (a) Batch conversion of EL over ZrO_2/SBA-15 after 6 h as a function of acid loading and GVL selectivity at 13 % isoconversion. (b) Corresponding TOF and GVL productivity as a function of acid loading after 2 h reaction.

creating Zr^{4+}-O^{2-} defect pairs. Such pairs are effective for -H abstraction and migration steps,[36] and also weaken the Lewis acidity of Zr^{4+} species which is expected to impact on 2-isopropanol activation and associated CTH.[37] The importance of Lewis and Brønsted acidity for the cascade conversion of EL to GVL is well-documented,[38-40] with the initial CTH step promoted by Lewis acid sites, and the subsequent lactonization-dealcoholisation step accelerated by Brønsted acid sites (**Scheme 3**). Only trace isopropyl levulinate from the competing transesterification of EL with 2-isopropanol was observed (**Figure S11**), suggesting a minor role for this indirect pathway to GVL. Isopropanol is reportedly less reactive towards the transesterification of alkyl levulinates than EtOH and MeOH.[24] Previously reported pathways of EL to GVL via angelica lactones[24, 25] were not identified in this study.

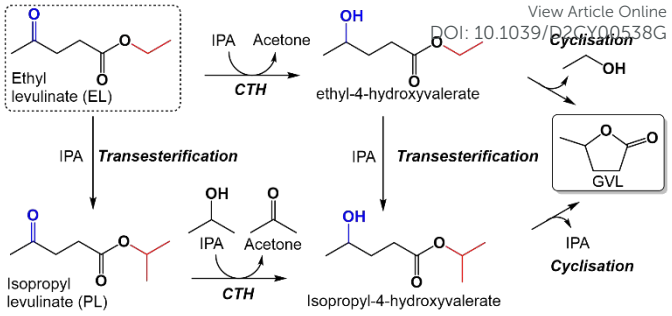

Scheme 3. Reaction pathways for the catalytic transfer hydrogenation of EL to GVL.

Continuous flow synthesis of γ-valerolactone from ethyl levulinate

Previous reports have demonstrated Zr-containing materials as effective catalysts for the vapour[24, 25, 41] and liquid phase[23, 27] continuous flow synthesis of GVL. The optimal catalyst from our batch studies, 11.6 wt% ZrO_2/SBA-15 was therefore selected for evaluation in a continuous flow, packed bed microreactor for the liquid phase transformation of EL to GVL. For safety reasons (to constrain the operating pressure ~5.5 bar), reactions were performed at 150 °C; an analogous batch reaction was also conducted at this lower temperature (**Figure S13**) to enable quantitative comparison (**Figure 4a**). With a residence time, τ, of 27.5 min (**Figure S14**), EL conversion averaged ~50 % over 6 h, approximately double that obtained in batch. The average GVL productivity in continuous flow approximately tripled relative to batch, being 5.2 vs 1.37 $mmol.g^{-1}.h^{-1}$, respectively. GVL selectivity was also slightly higher in a flow configuration (61 % versus 55 %). Consequently, the cumulative GVL yield over 6 h was 3.6 times greater in flow (2.78 mmols) than batch (0.77 mmols). Analysis of the corresponding acetone by-product of the initial CTH step, revealed that this was almost stoichiometric with GVL for continuous flow synthesis (as expected if the second dealcoholisation/cyclisation step proceeds efficiently).

In contrast, the acetone yield in batch was almost double that of GVL **(Figure S15)**, suggesting sluggish kinetics for conversion of the hydroxyvalerate intermediate to GVL; this may reflect associative desorption of hydrogen adatoms liberated by dehydrogenation of high surface concentrations of 2-isopropanol possible during batch operation. The catalytic advantage of flow operation was diminished at shorter residence time (τ=17.5 min) (**Figure S16**), with average EL conversion falling to 20 %, accompanied by a slight decrease in GVL selectivity; resulting in a cumulative GVL yield of 1.82 mmols, with a GVL selectivity of approximately 56% **(Figure 4b)**. The latter changes are expected, and attributed to the shorter time available for the reaction of EL, and reactively-formed hydroxyvalerate intermediate, over the catalyst bed.

Enhanced EL reactivity in flow was also apparent from the greater turnover frequency (TOF) than that in batch (**Figure 5**), although significant deactivation, from an initial high of 23 h^{-1} to a plateau of 7 h^{-1}, was observed over the course of reaction in the former case. This deactivation was accompanied by a dramatic rise in selectivity to GVL (**Figure S14**) suggesting that: (i) the

View Article Online
DOI: 10.1039/D2CY00538G

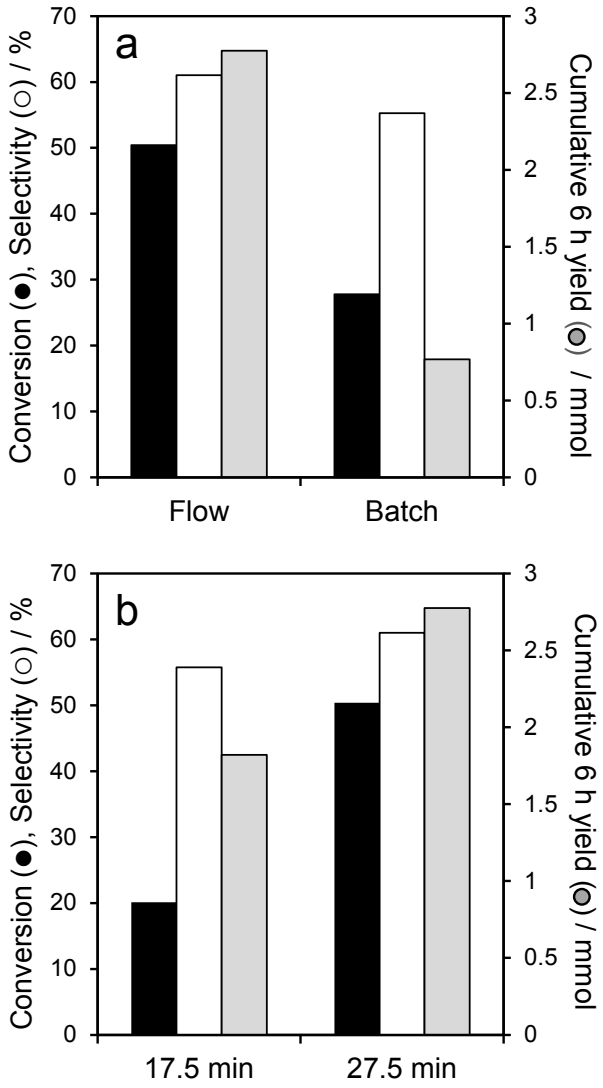

Figure 4. (a) Comparison of flow and batch EL transformation GVL catalysed by 11.6 wt% Zr/SBA-15. (b) Influence of residence time of flow reaction. Reaction conditions: 100 mg catalyst, 150 °C, liquid stream of ethyl levulinate (0.25M) and 2-isopropanol.

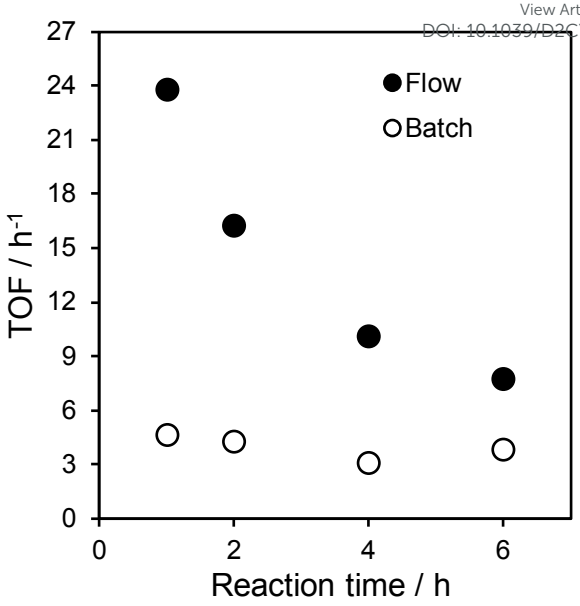

Figure 5. Comparison of batch and flow turnover frequency (TOF) for the conversion of EL to GVL employing 11.6 wt% Zr/SBA-15. Reaction conditions: 100 mg catalyst, 150 °C, τ = 27.5 min, liquid stream of ethyl levulinate (0.25 M) and 2-isopropanol.

as-prepared catalyst contains a distribution of Lewis acid sites, with the strongest sites rapidly poisoned by reactively-formed products, slowing the first CTH step; and (ii) the Brønsted acid catalysed second step is slower than that of CTH over strong acid sites, and efficient removal of accumulated ethyl-4-hydroxyvalerate only occurs after these strong sites are poisoned. Despite this on-stream deactivation, TOFs for flow operation remained higher than batch (3-4 h^{-1}) over the course of 6 h. Similar on-stream catalyst deactivation was reported for the liquid phase flow reaction of butyl levulinate, wherein a comparable decline in GVL productivity occurred before stabilising.[23] This deactivation is most likely a consequence of catalyst poisoning through gradual site-blocking of Lewis acid sites by reactively-formed GVL and/or acetone.

Optimisation studies (see ESI) were performed to explore the impact of reaction temperature and EL concentration on reactivity. No EL conversion was observed at 110 °C (**Figure S17a**), with an apparent activation energy of 90 $kJ.mol^{-1}$ (**Figure S17b**) for reaction between 130-150 °C, somewhat higher than the 72 $kJ.mol^{-1}$ reported by Lai et al for the batchwise CTH of EL to GVL over graphene oxide supported ZrO_2 between 140-180 C.[29] GVL selectivity was temperature independent, consistent with previous studies by Dumesic and co-workers who observed no loss in GVL selectivity <220 °C.[23] Selectivity to GVL was also independent of EL concentration, likely reflecting the large excess of 2-isopropanol solvent/reactant (**Figure S18**). Doubling the EL concentration to 0.48 M enhanced the GVL yield by ~34 %, demonstrating the presence of additional underutilised active sites under the standard reaction condition (0.25 M EL). Decreasing the EL concentration was detrimental to both EL conversion and GVL yield, suggesting that EL is unable to compete effectively with 2-isopropanol and adsorb at active ZrO_2 sites at low these concentrations.

Spiking studies with GVL and acetone were therefore conducted under different conditions (see ESI) to assess their potential roles as catalyst poisons. In the case of GVL (**Figure 6**), comparison of the average EL conversion after 2 h reveals that pre-treatment of the packed catalyst bed with GVL for 30 min at 150°C prior to reaction decreased EL conversion by 20 %. The impact of GVL was even more pronounced when continuously introduced into the EL reaction stream; activity halved under stoichiometric operation (GVL:EL molar ratio = 1) and by 70 % when GVL was present in excess (GVL:EL = 5). Removal of GVL from the reaction stream almost fully recovered the original catalytic activity, consistent with competition between EL and reversibly adsorbed GVL for Lewis acid sites. Similar spiking studies for acetone (**Figure S19**) revealed a far weaker impact on activity. These observations are consistent with the on-stream deactivation apparent in **Figure 5**,

with the deactivation rate highest at the start of reaction wherein GVL productivity is greatest.

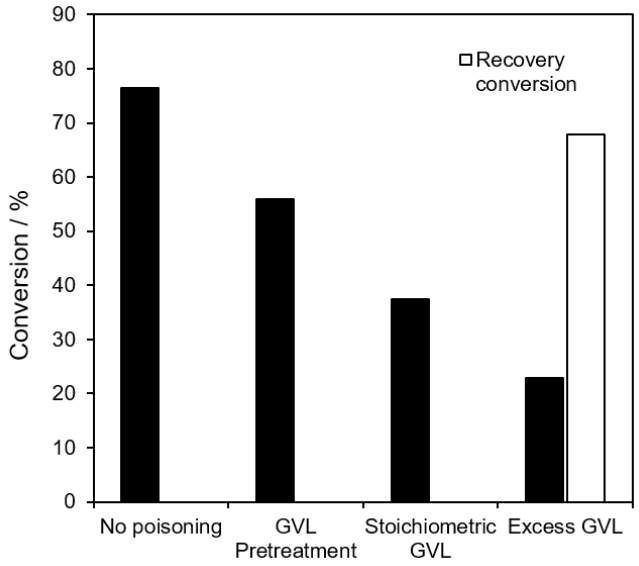

Figure 6. Comparison of EL conversion after 2 h reaction over 11.6 wt% Zr/SBA-15 in the absence of GVL and after: 30 min pretreatment in pure GVL at 150°C; addition of stoichiometric GVL; addition of excess (5:1) GVL; or addition of excess GVL and subsequent removal. Reaction conditions: 100 mg catalyst, 150 °C, τ = 27.5 min, 0.25 M EL in a 2-isopropanol feedstream.

Post-reaction characterisation of 11.6 wt% Zr/SBA-15 following continuous flow EL conversion to GVL under standard reaction conditions confirmed significant accumulation of organic adsorbates. The surface carbon content increased from 5.9 atom% in the as-prepared catalyst to 17.8 atom% after reaction (**Table S2**). Fitting of the high-resolution C 1s XP spectra is consistent with the presence of surface alcohol and carbonyl species (**Table S2**), evidenced by peaks at 286.1 eV and 288.1 eV binding energies **(Figure S20)**, respectively.[42, 43] The presence of surface carbonyls post-reaction is in accordance with the preceding poisoning of Lewis acid sites by reactively-formed GVL (and to a lesser extent) acetone. Catalyst stability was explored by performing three consecutive 6 h reactions, with pure 2-isopropanol flowed over the catalyst at 150 °C for 1 h between each reaction. Although each mild, in-situ regeneration treatment afforded a ~20 % enhancement in EL conversion, the enhancement was short-lived, with activity returning after an hour to track the original deactivation profile (**Figure S21**). Elemental analysis (ICP-OES) of the reactor exit stream showed this deactivation was not associated with Zr leaching, and is hence attributed to adsorption of strongly bound oxygenates.

Conclusions

Acid properties of conformal ZrO_2 adlayers dispersed over a mesoporous SBA-15 silica support were systematically tuned to optimise the cascade transformation of ethyl levulinate (EL) to γ-valerolactone (GVL). Lewis and Brønsted character are both required for efficient EL conversion and high selectivity to the desired GVL product. At low ZrO_2 surface coverages, Lewis acidity dominates, with significant Brønsted acidity only emerging on completion of a ZrO_2 monolayer (corresponding to 11.6 wt% Zr). Cooperativity between Lewis acid-base pairs and Brønsted sites in the ZrO_2 monolayer is proposed responsible for increased activity and GVL selectivity (which reaches 70 %). Continuous flow operation offers faster EL conversion and higher GVL selectivity, attributed to reversible poisoning of Lewis acid sites, responsible for the catalytic transfer hydrogenation of EL to the hydroxyvalerate intermediate, by reactively-formed GVL. In the absence of this self-poisoning, Brønsted acid catalysed dealcoholisation and cyclisation of the hydroxyvalerate intermediate to GVL is rate-limiting. Flow synthesis increases the cumulative GVL yield by four-fold relative to batchwise operation at 150 °C; flow chemistry offers significant performance improvement and flexibility in reactor operation for biomass valorisation.

Author Contributions

Amin Osatiashtiani (Investigation, methodology, formal analysis), Samantha A. Orr (Investigation, formal analysis, writing - original draft), Lee J. Durndell (Investigation, formal analysis), Irene Collardo Garcia (Investigation, formal analysis), Andrea Merenda (Investigation, formal analysis), Adam F. Lee (Resources, supervision, funding acquisition, writing – review and editing) and Karen Wilson (Resources, supervision, funding acquisition, writing – review and editing).

Conflicts of interest

There are no conflicts to declare.

Acknowledgements

We thank the Australian Research Council for financial support (DP200100204, DP200100313 and LE210100100), and the RMIT Microscopy and Microanalysis Facility for access to analytical services.

Notes and references

1. T. Werpy and G. Petersen, in *Top Value Added Chemicals from Biomass*, ed. D. o. Energy, U. S., 2004.
2. J. J. Bozell and G. R. Petersen, *Green Chemistry*, 2010, **12**.
3. C. O. Tuck, E. Perez, I. T. Horvath, R. A. Sheldon and M. Poliakoff, 2012, **337**, 695-699.
4. D. Haldar and M. K. Purkait, *Process Biochemistry*, 2020, **89**, 110-133.
5. I. T. Horváth, H. Mehdi, V. Fábos, L. Boda and L. T. Mika, *Green Chem.*, 2008, **10**, 238-242.
6. D. M. Alonso, S. G. Wettstein and J. A. Dumesic, *Green Chemistry*, 2013, **15**.
7. X. Tang, X. Zeng, Z. Li, L. Hu, Y. Sun, S. Liu, T. Lei and L. Lin, *Renewable and Sustainable Energy Reviews*, 2014, **40**, 608-620.
8. K. Yan, Y. Yang, J. Chai and Y. Lu, *Applied Catalysis B: Environmental*, 2015, **179**, 292-304.

9. Z. Zhang, *ChemSusChem*, 2016, **9**, 156-171.
10. L. Ye, Y. Han, J. Feng and X. Lu, *Industrial Crops and Products*, 2020, **144**.
11. F. Kerkel, M. Markiewicz, S. Stolte, E. Müller and W. Kunz, *Green Chemistry*, 2021, **23**, 2962-2976.
12. L. E. Manzer, *Applied Catalysis A: General*, 2004, **272**, 249-256.
13. L. Bui, H. Luo, W. R. Gunther and Y. Roman-Leshkov, *Angew Chem Int Ed Engl*, 2013, **52**, 8022-8025.
14. J. Iglesias, J. A. Melero, G. Morales, M. Paniagua, B. Hernández, A. Osatiashtiani, A. F. Lee and K. Wilson, *Catalysis Science & Technology*, 2018, **8**, 4485-4493.
15. T. Zhang, Y. Lu, W. Li, M. Su, T. Yang, A. Ogunbiyi and Y. Jin, *International Journal of Hydrogen Energy*, 2019, **44**, 14527-14535.
16. Y.-B. Huang, T. Yang, Y.-J. Luo, A.-F. Liu, Y.-H. Zhou, H. Pan and F. Wang, *Catalysis Science & Technology*, 2018, **8**, 6252-6262.
17. W. R. Wright and R. Palkovits, *ChemSusChem*, 2012, **5**, 1657-1667.
18. K. Yan, T. Lafleur, G. Wu, J. Liao, C. Ceng and X. Xie, *Applied Catalysis A: General*, 2013, **468**, 52-58.
19. M. G. Al-Shaal, W. R. H. Wright and R. Palkovits, *Green Chemistry*, 2012, **14**.
20. P. P. Upare, J.-M. Lee, D. W. Hwang, S. B. Halligudi, Y. K. Hwang and J.-S. Chang, *Journal of Industrial and Engineering Chemistry*, 2011, **17**, 287-292.
21. Z. Yu, X. Lu, J. Xiong, X. Li, H. Bai and N. Ji, *ChemSusChem*, 2020, **13**, 2916-2930.
22. A. Shivhare, A. Kumar and R. Srivastava, *ChemCatChem*, 2020, **13**, 59-80.
23. M. Chia and J. A. Dumesic, *Chem Commun (Camb)*, 2011, **47**, 12233-12235.
24. T. Tabanelli, E. Paone, P. Blair Vásquez, R. Pietropaolo, F. Cavani and F. Mauriello, *ACS Sustainable Chemistry & Engineering*, 2019, **7**, 9937-9947.
25. P. B. Vásquez, T. Tabanelli, E. Monti, S. Albonetti, D. Bonincontro, N. Dimitratos and F. Cavani, *ACS Sustainable Chemistry & Engineering*, 2019, **7**, 8317-8330.
26. Y. Kuwahara, W. Kaburagi, Y. Osada, T. Fujitani and H. Yamashita, *Catalysis Today*, 2017, **281**, 418-428.
27. N. Lázaro, A. Franco, W. Ouyang, A. Balu, A. Romero, R. Luque and A. Pineda, *Catalysts*, 2019, **9**.
28. X. Tang, H. Chen, L. Hu, W. Hao, Y. Sun, X. Zeng, L. Lin and S. Liu, *Applied Catalysis B: Environmental*, 2014, **147**, 827-834.
29. J. Lai, S. Zhou, X. Liu, Y. Yang, J. Lei, Q. Xu and D. Yin, *Catalysis Letters*, 2019, **149**, 2749-2757.
30. R. Gerardy, D. P. Debecker, J. Estager, P. Luis and J. M. Monbaliu, *Chem Rev*, 2020, **120**, 7219-7347.
31. M. Baumann, T. S. Moody, M. Smyth and S. Wharry, *Organic Process Research & Development*, 2020, **24**, 1802-1813.
32. T. Tabanelli, P. Vásquez, E. Paone, R. Pietropaolo, N. Dimitratos, F. Cavani and F. Mauriello, presented in part at the Proceedings of 1st International Electronic Conference on Catalysis Sciences, 2020.
33. J. M. Tukacs, Á. Sylvester, I. Kmecz, R. V. Jones, M. Óvári and L. T. Mika, *Royal Society Open Science*, 2019, **6**, 182233.
34. G. Morales, A. Osatiashtiani, B. Hernandez, J. Iglesias, J. A. Melero, M. Paniagua, D. R. Brown, M. Granollers, A. F. Lee and K. Wilson, *Chem Commun (Camb)*, 2014, **50**, 11742-11745.
35. D. Zhao, J. Feng, Q. Huo, N. Melosh, G. H. Fredrickson, B. F. Chmelka and G. D. Stucky, *Science*, 1998, **279**, 548-552.
36. K. T. Jung and A. T. Bell, *Journal of Molecular Catalysis A: Chemical*, 2000, **163**, 27-42.
37. H. Jahangiri, A. Osatiashtiani, J. A. Bennett, M. A. Isaacs, S. Gu, A. F. Lee and K. Wilson, *Catalysis Science & Technology*, 2018, **8**, 1134-1141.
38. N. Ji, X. Diao, Z. Yu, Z. Liu, S. Jiang, X. Lu, C. Song, Q. Liu, D. Ma and C. Liu, *Catalysis Science & Technology*, 2021, **11**, 5062-5076.
39. Y. Kuwahara, H. Kango and H. Yamashita, *ACS Sustainable Chemistry & Engineering*, 2016, **5**, 1141-1152.
40. F. Li, L. J. France, Z. Cai, Y. Li, S. Liu, H. Lou, J. Long and X. Li, *Applied Catalysis B: Environmental*, 2017, **214**, 67-77.
41. S. S. Enumula, V. R. B. Gurram, M. Kondeboina, D. R. Burri and S. R. R. Kamaraju, *RSC Advances*, 2016, **6**, 20230-20239.
42. E. Bayram, G. Yilmaz and S. Mukerjee, *Applied Catalysis B: Environmental*, 2016, **192**, 26-34.
43. F. Wan, B. Yang, J. Zhu, D. Jiang, H. Zhang, Q. Zhang, S. Chen, C. Zhang, Y. Liu and Z. Fu, *Green Chemistry*, 2021, **23**, 3428-3438.